REMOTE SENS. ENVIRON. 48:231–244 (1994)

Change-Vector Analysis in Multitemporal Space: A Tool To Detect and Categorize Land-Cover Change Processes Using High Temporal-Resolution Satellite Data

Eric F. Lambin[*] *and Alan H. Strahler*[†]

Analysis of change vectors in the multitemporal space, applied to multitemporal local area coverage imagery obtained by the Advanced Very-High Resolution Radiometer on NOAA-9 and NOAA-11 orbiting platforms, clearly reveals the nature and magnitude of land-cover change in a region of West Africa. The change vector compares the difference in the time-trajectory of a biophysical indicator, such as the normalized difference vegetation index, for two successive time periods, such as hydrological years. In establishing the time-trajectory, the indicator is composited for each pixel in a registered multidate image sequence. The change vector is simply the vector difference between successive time-trajectories, each represented as a vector in a multidimensional measurement space. The length of the change vector indicates the magnitude of the interannual change, while its direction indicates the nature of the change. A principal components analysis of change vectors for a Sudanian-Sahelian region in West Africa shows four major classes of change magnitude and four general contrasting types of change. Scene-specific changes, such as reservoir water level storage changes, are also identified. The technique is easily extended to other biophysical parameters, such as surface temperature, and can incorporate noneuclidean distance measures. Change vector analysis is being developed for application to the land-cover change product to be produced using NASA's Moderate-Resolution Imaging Spectroradiometer instrument, scheduled for flight in 1998 and 2000 on EOS-AM and -PM platforms.

[*] Institute for Remote Sensing Applications, Joint Research Center, Ispra, Italy.
[†] Department of Geography, Boston University.
Address correspondence to Eric F. Lambin, TP 440, Institute for Remote Sensing Applications, Joint Research Center, 7-21020 Ispra (Varese), Italy.
Received 18 March 1993; revised 24 July 1993.

0034-4257/94/$7.00

655 Avenue of the Americas, New York, NY 10010

INTRODUCTION

Land-cover, and human or natural alterations of land-cover, play a major role in global-scale patterns of climate and biogeochemistry of the earth system. The land surface has considerable control on the planet's energy balance, biogeochemical cycles, and hydrologic cycle, which in turn significantly influence the climate system. Variations in vegetation cover and, hence, physical characteristics of the land surface such as albedo, emissivity, roughness, and plant transpiration also generate variations of weather and climate by altering the hydrological cycle and land–atmosphere energy fluxes. Global assessment of the changes in physical characteristics of land-cover is therefore a fundamental input for models of global climate and terrestrial hydrology. While some of these changes in land-cover are caused by natural processes, such as long-term changes of the climate due to astronomical causes, or shorter-term vegetation successions and geomorphological processes, human activity increasingly modifies surface cover through direct actions, such as deforestation, farming activities, urbanization, or indirectly through man-induced climatic change. The importance of mapping, quantifying, and monitoring the changes in physical characteristics of land-cover have been widely recognized in the scientific community as a key element in the study of global change (e.g., IGBP, 1990; Anonymous, 1992; Henderson-Sellers and Pitman, 1992). This article, presents a change detection method designed for high temporal resolution data, such as those of NOAA's Advanced Very High Resolution Radiometer (AVHRR), in order to address the need for global data on the nature and magnitude of processes of land-cover change. This method should detect areas of change and categorize the type of change processes occurring. It is being developed in the context of the

land-cover change product to be produced using NASA's Moderate Resolution Imaging Spectroradiometer (MODIS), an instrument to be flown on the EOS-AM and PM platforms in 1998 and 2000.

CHANGE DETECTION METHOD

Classic digital change detection techniques using remotely sensed data are based on the comparison of sequential data taken from the same area and on the display of the changes and their locations. There are two approaches to change detection (Malila, 1980; Colwell and Weber, 1981): comparative analysis of independently-produced classifications, and simultaneous analysis of multitemporal data. The first approach has significant limitations. The comparison of land-cover classifications for different dates does not allow the detection of subtle changes within a land-cover class. Also, the change map product of two classifications exhibits accuracies similar to the product of multiplying the accuracies of each individual classification (Stow et al., 1980).

The land-cover change detection approach discussed in this article utilizes the second approach. Rather than analyzing isolated dates from two separate time periods, it is based on a comparison of the temporal development curve, or time-trajectory, for successive years of indicators derived from AVHRR data, such as vegetation indices, surface temperature, or spatial structure. Other researchers have shown that a high temporal frequency of measurement, which is a characteristic of the AVHRR sensor, allows the characterization of vegetation types by analysis of the seasonal or phenological variations of these spectral indicators (Thomas and Henderson-Sellers, 1987; Townshend et al., 1991). It can therefore be expected that the interannual comparison of temporal development curves will also be required to detect most types of land-cover change processes.

When the time trajectory of one or several indicators over a particular pixel departs from that expected for that pixel, a process of land-cover change can be detected. The expected time trajectory can be derived from the past history of that pixel. In addition to allowing an unambiguous detection of abrupt changes in land-cover types, this multitemporal approach is more sensitive to subtle changes in seasonality, primary productivity, vegetation phenology, and ecosystem dynamic than the more classic approaches, for which only a few isolated dates from different years or seasons are compared. In that latter case, not only the rich seasonal information of remotely sensed data is ignored, but also an obvious undersampling of the temporal series hinders the change detection accuracy. This undersampling is particularly problematic when dealing with abrupt and sometimes brief ecological events such as vegetation stress, flooding, burning, or dry spells. In that case, the few dates on which the interannual comparison is based can give a poor representation of the real land-cover types and lead to the detection of spurious or ambiguous changes.

Singh (1989) reviews a variety of procedures and applications of digital change detection using high spatial resolution data. Other studies, based on coarser scale AVHRR data, have used annual integrated or isolated dates of vegetation index data (or original Channels 1 and 2) to document the interannual variations in primary production in the Sahel (Tucker et al., 1986; Hellden and Eklundh, 1988; Hellden, 1991; Tucker et al., 1991) and to quantify large-scale tropical deforestation (Tucker et al., 1984; Nelson and Holben, 1986; Woodwell, 1987; Malingreau et al., 1989). While the procedures used in these studies are appropriate to detect abrupt land-cover changes such as forest clearing, biomass burning, or the impact of a severe drought, the detection of more subtle forms of changes, such as those associated with climate change or with slow rates of land degradation, requires a more sophisticated approach. The quantitative evaluation of differences in seasonal development curves of remotely sensed data has not yet been systematically applied to detect changes in land-cover. However, this criterion has been used qualitatively to detect the damage caused by a drought and a large-sclae fire on tropical forest in eastern Kalimantan (Malingreau et al., 1985) and the impact of drought on rice growing areas and forests in Asia (Malingreau, 1986).

MULTITEMPORAL CHANGE VECTOR

Analysis of Temporal Series

The comparison on an annual basis of vegetation index or surface temperature temporal development curves, on a pixel-by-pixel basis, requires the analysis of time-trajectory shapes every year, for all pixels. This should take place after filtering the multitemporal data for noise introduced by atmospheric effects, sensor calibration, and variations in viewing geometry. Various attempts have been made to develop mathematical expressions that fit vegetation development curves, using logistic or exponential expressions (Badhwar and Henderson, 1985), using a combination of those for different phases of the radiometric evolution of a vegetative cover (Baret and Guyot, 1986), or jointly using the results of the theories of generalized shift and of projection pursuit (Antonovski et al., 1991). Other studies have used a few simple parameters to characterize the evolution in time of vegetation indices: the onset of greenness, the peak of greenness, the length of growing season, the integrated vegetation index, the amplitude of the variation, etc. (Odenweller and Johnson, 1984; Malingreau, 1989; Lloyd,

1990; Loveland et al., 1991). Samson (1993) proposes a skew index and a range index to characterize the shape of the seasonal profile of vegetation indices. Tucker et al. (1985) used the information from the first two principal components of annual NDVI time series as measures of mean annual NDVI value and seasonality to classify the time-profiles of land-cover types on a continental scale in Africa. For our objective of comparing successive temporal profiles to detect subtle land-cover changes, a method of analysis which captures the maximum detail contained in the time-trajectory of the indicator is needed.

The seasonal dynamic of a remotely sensed indicator can be represented by a point in a multidimensional space, with the number of dimensions of this space corresponding to the number of observations. These observations will either correspond to the maximum values of the indicator for prespecified compositing periods, or the results of a sampling through time of a continuous function that describes the shape of the time-trajectory of the indicator. If we assume monthly-composited data or a monthly rate of sampling, 12 successive images will be available. The value taken by the indicator under consideration can be represented, for each pixel, by a point in the 12-dimensional temporal space defined by the vector:

$$\mathbf{p}(i,y) = \begin{bmatrix} \mathbf{I}(t_1) \\ \mathbf{I}(t_2) \\ \cdots \\ \cdots \\ \mathbf{I}(t_n) \end{bmatrix},$$

where $\mathbf{p}(i,y)$ is the multitemporal vector for pixel i and the year y, and **I**'s are the values of the indicator under consideration for pixel i at the time periods t_1 to t_n, n being the number of time dimensions. The magnitude of this vector, $|\mathbf{p}|$, measures the accumulated value of the indicator through the year. The direction of this vector, measured by the direction angles of **p**, is a synthetic quantifier of the seasonal pattern of the indicator, that is, the shape of the curve.

Figure 1 presents a simple example. This figure compares the vegetation index vectors for 1 year, for pixels corresponding to idealized desert and savanna classes, assuming only two periods of observation a year—winter and summer. [The shape of these curves generally follow Tucker et al. (1985) and Townshend et al. (1987).] The magnitude of the vectors, which is proportional to the absolute values of the axis coordinates, represents the cumulative vegetation index for that year. This annual integrated vegetation index has been related to the total dry-matter accumulation (Tucker et al., 1983), the net primary productivity (Sellers, 1985; Tucker and Sellers, 1986; Goward et al., 1985; Box et al., 1989), and actual evapotranspiration (Box et al., 1989; Cihlar et al., 1991) of the land cover. The direction of the vectors, which depends on the relative values of the axis coordinates, quantifies the seasonal variations of the vegetation index. These variations can be interpreted in terms of vegetation phenology (Tucker et al., 1985; Justice et al., 1985; Goward et al., 1985), length of growing season (Justice et al., 1986), or, at a coarser spatial scale, biome seasonality and dynamics (Malingreau et al., 1985).

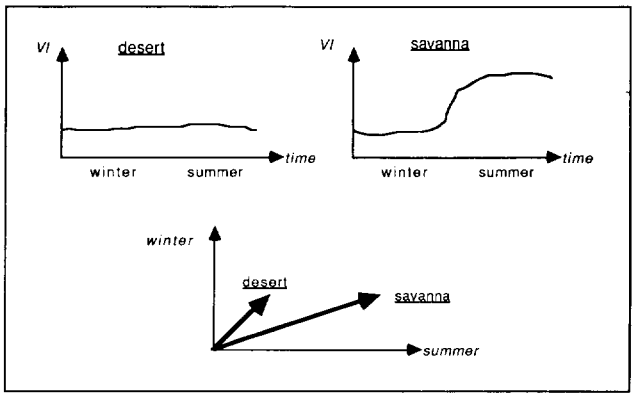

Figure 1. Examples of multitemporal vectors for two simulated land-cover types.

Change Vector

Every year, the coordinates of the position of any pixel in the multidimensional temporal space can be observed. Any change in accumulated value and/or in seasonal dynamic of the indicator between successive years will result in a displacement of the pixel's point in the multidimensional space. This difference in position can be described by a change vector:

$$\mathbf{c}(i) = \mathbf{p}(i,y) - \mathbf{p}(i,z),$$

where $\mathbf{c}(i)$ is the change vector for pixel i between the years y and z. Change vector analysis has been applied earlier in the multispectral space (Malila, 1980; Colwell and Weber, 1981; Virag and Colwell, 1987). In this article, we apply the same concept to the multitemporal space—that is, the multispectral observation vectors are replaced by time-series observation vectors of an indicator variable measured for different years.

The magnitude of the change vector, $|\mathbf{c}|$, calculated as the Euclidean distance between the two positions, measures the intensity of the change in land cover. The direction of the change vector, measured by the direction angles of **c**, indicates the nature of the land-cover change process. Figure 2 illustrates this point. This figure presents simplistic simulations of two land-cover change processes measured by a vegetation index, assuming two observation periods a year. In the first example, an idealized process of desertification, the degradation of the vegetation cover from a wooded savanna to a steppe leads to a decrease in the cumulative value of the vegetation index, the phenology of the two covers remaining unaltered. The second example

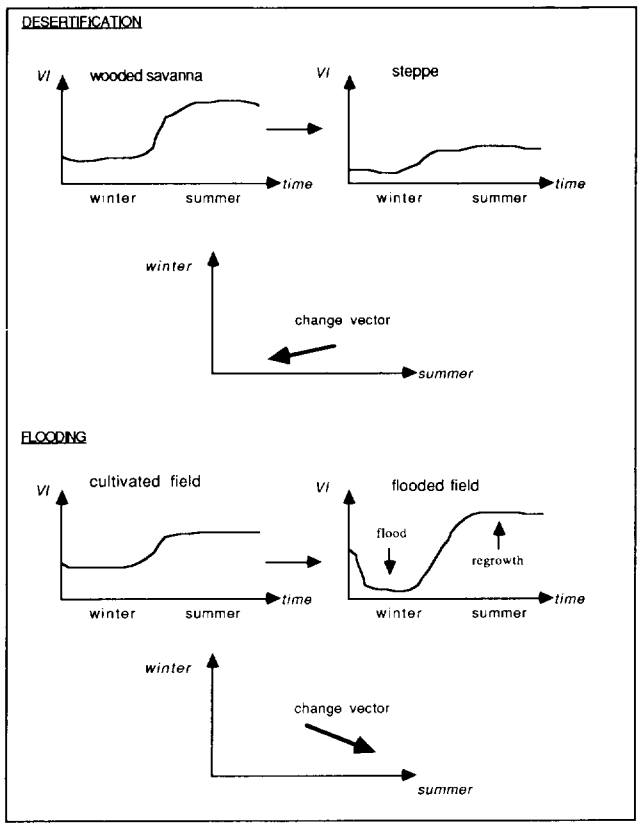

Figure 2. Examples of change vectors for two simulated land-cover change processes.

represents simplistically the impact of seasonal floods in a delta region. During the first part of the year, the vegetation index is depressed by the standing water and high soil moisture, which absorb near infrared radiation. During the second season, an active vegetation regrowth is stimulated due to the new silt deposited and a greater water availability, which leads to a higher than usual increase in vegetation index value. This figure illustrates that the magnitude of the change vector increases with the intensity of the land-cover change. Moreover, for these two examples, the direction of the change vector varies with the type of change process. This allows a categorization of change processes according not only to their impact on the annualized integrated vegetation index value but also to their effect on the seasonality of the indicator.

In general, the change vector will be oriented along an axis going through the origin when the change processes do not alter the seasonal pattern of the indicator, that is, if only the cumulative value is changed. (Since this direction corresponds to a diagonal connecting the origin with the opposite corner of the parallelepiped defined by the vector $\mathbf{p}$, we refer to this direction as along the diagonal.) In contrast, when the change processes modify the seasonality of the indicator, the direction of the change vector will be oriented along an off-diagonal direction. The multidimensional temporal space can therefore be segmented into a set of basic directions corresponding to certain categories of land-cover change processes. This "compass-card" of temporal changes can serve as a basis for a categorization of change processes, such as permanent clearing of vegetation, changes from seasonal to perennial crops, soil degradation, irrigation of drylands, etc. This approach has several advantages: It provides a quantifier of the intensity of change, it allows a characterization of the nature of the change process, it is based on the history of each particular pixel, and it involves simple mathematical methods.

High Interannual Variability of Ecosystem Conditions

Some ecosystems, such as those of semiarid regions, are characterized by a large interannual variability in climatic conditions, leading to large interannual variations in vegetation productivity. It might therefore be difficult to distinguish the trends of land-cover changes caused by human disturbances or by long-term changes in climatic conditions from the noise created by aperiodic and recurring rainfall shortages. The multitemporal change vector method can be adapted to allow this less-significant interannual variability of vegetation condition to be taken into account. If long-term data on the spectral behavior of every pixel have been collected and archived, the current position of one pixel in the multidimensional space can be compared with the set of positions of that pixel during the previous years of observation. If there is a large number of these past records, the Mahalanobis distance can be used in place of the Euclidean distance.

In the formulation of the Mahalanobis distance, the distance between a point, defined by the vector $\mathbf{p}_i$, and the mean of a set of other points is modulated with the covariance matrix, which confers a degree of directional sensitivity to the measure:

$$d(\mathbf{p}_i,\mathbf{m})^2 = (\mathbf{p}_i - \mathbf{m})^t \boldsymbol{\Sigma}^{-1} (\mathbf{p}_i - \mathbf{m}),$$

where $\mathbf{m}$ and $\boldsymbol{\Sigma}$ are the mean vector and covariance matrix of the archived data. Therefore, the amplitude of a change in a certain direction is weighted by the probability that the natural interannual variability of the climate leads to a change in that direction, this probability being inferred from the covariance matrix of past observations. In semiarid regions for instance, the variability of vegetation conditions is restricted to the rainy season, only 3–4 months a year. Thus, in normal conditions, the covariance will be high along these temporal dimensions and very low along the other dimensions corresponding to the dry season. Since this study examines only two years of multitemporal data, a covariance matrix is not available. However, the use of Mahalanobis distance could be easily explored as longer datasets are accumulated.

TEST OF THE METHOD

The change detection method described in the previous section were tested with AVHRR data over an area in West Africa. However, the AVHRR GAC product suffers from spatial sampling problems (Justice et al., 1989; Belward and Lambin, 1990), which decrease the accuracy of multitemporal comparisons. The global vegetation index data set (GVI), produced by sampling and compositing of the GAC data, have further degraded the original observations (Goward et al., 1991). Therefore, 1.1 km resolution AVHRR LAC / HRPT data were selected. Our tests have been conducted using the normalized difference vegetation index (NDVI), the most widely used vegetation index in coarse scale studies.

Study Area

A subscene of 512 × 512 pixels of LAC AVHRR data covering a region in West Africa across Mali, Senegal, and Guinea was selected for our test (Fig. 3) (Grégoire, 1990). This area includes several watersheds from the Niger, Senegal, and Gambia rivers systems as well as the northern edge of the Fouta Djallon, southwest of the scene. Precipitation varies from about 1800 mm in the Fouta Djallon to 750 mm in the north of the scene. The rainy season normally occurs from June to early October, but is shorter and starts later in the north of the scene. The area belongs to the Sudanian phytogeographic zone and, in the northern part, to the Sahelian domain. In the south, the vegetation type is open forest dominated by deciduous and semideciduous species with an herbaceous stratum, ranging to tree and shrub savannas. To the north, the herbaceous stratum dominates the landscape. The combined effect of vegetation type and climatological zoning leads to north–south variations in vegetation phenology. Vegetation senescence occurs earlier and more rapidly on the northern grass savanna than on the southern woody savanna and open forest. The patterns of vegetation growth vary similarly with vegetation types and the timing of the rains (ORSTOM, 1991). These geographic variations in vegetation response have been analyzed by Grégoire (1990) using AVHRR data in the thermal domain (Channel 3) and in the reflective domain (NDVI) for a few selected dates.

There are three main processes of interannual land-cover change acting in the region. First, the timing of vegetation activity varies from one year to another as a result of variations in rainfall distribution. These changes are nonpermanent and are driven by the interannual climatic variability. Second, changes in vegetation types occur as a result of human activity or longer-term climatic changes. These changes are not well documented for the region and probably occur at a slow rate. Third, biomass burning is an important process of land-cover change and ecological degradation that affects the area. Bush fire activity is maximum from the end of October to early January.

Figure 3. Location of the study area.

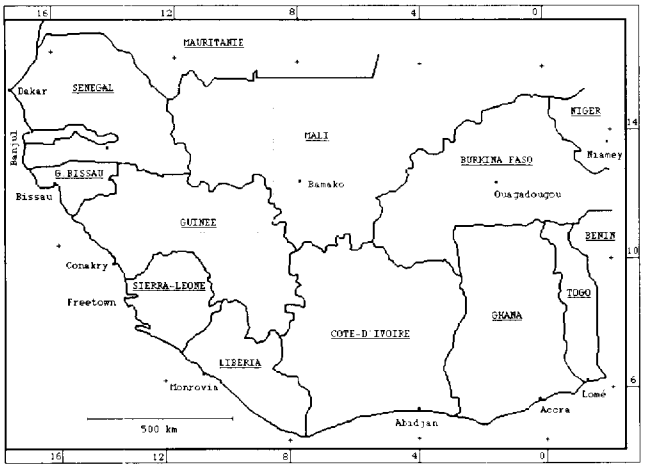

Meteorological Data

Land-cover changes were analyzed between two hydrological years (from July to June 1987 / 88 and 1988 / 89). Monthly meteorological and hydrological data for these two years were available for three different stations along the Faleme watershed, which occupies a large part of the AVHRR subscene. The rainfall and hydrological data reveal the following interannual differences (see Table 1 and Fig. 4) (ORSTOM, 1991):

1. The annual precipitation values for the two years were approximately equal for the three stations but, for both years, lower than the long-term average.
2. The second hydrological year (1988 / 89) was characterized by an earlier and more intense start of the rainy season, with a maximum in precipitation occurring in July compared to August for the first year. These different rainfall distributions are expected to lead to differences in the timing of vegetation growth.
3. During the second hydrological year (1988 / 89), the month of October, at the end of the rainy season, was drier than the same period for the first year. This also contributed to an earlier senescence of vegetation at the begin of the second year's dry season as compared to the first year.

It should also be noted that a high spatial variability in rainfall distribution is typical of Sahelo-Sudanian regions (Flitcroft et al., 1989). The network of meteorological stations is too sparse to grasp accurately the spatial variations in rainfall distribution throughout the area.

Remotely Sensed Data

The multiyear AVHRR LAC multitemporal data used in this study were assembled and preprocessed by the

Table 1. Monthly and Annual Precipitation (mm) at Three Stations in the Faleme Watershed

	Precipitation (mm)					
	Kidira (North)		*Gourbassy (Center)*		*Fadougou (South)*	
	1987/88	*1988/89*	*1987/88*	*1988/89*	*1987/88*	*1988/89*
May	33.6	34.0	52.9	37.3	79.2	26.9
June	90.7	101.9	101.8	149.2	126.3	178.9
July	176.5	239.5	210.3	259.3	228.1	284.1
August	243.8	192.6	266.1	196.6	298.9	241.6
September	159.6	204.9	178.4	219.2	185.2	217.6
October	85.3	13.3	69.1	9.4	82.1	14.6
November	0.3	11.3	0.6	19.4	0.9	29.4
December	0.0	0.0	0.0	0.0	0.0	0.0
January	0.0	0.0	0.0	0.0	0.0	0.0
February	0.0	1.3	0.0	2.2	0.0	3.4
March	0.0	2.8	0.0	4.7	0.0	7.2
April	11.4	2.0	15.4	3.4	15.0	5.1
Annual	**801.2**	**803.6**	**894.6**	**900.6**	**1015.7**	**1008.9**

Monitoring Tropical Vegetation group, at the Joint Research Center (Ispra, Italy). Data were acquired by the NOAA-9 and, after November 1988, NOAA-11 satellites. NOAA-11 has an earlier equatorial crossing time than NOAA-9. The resulting change in solar zenith angles, as well as differences in prelaunch calibration characteristics, were compensated for when calculating apparent at-satellite reflectances, by using corrections for the sun-zenith angle, the sun–earth distance and the spectral response function of the sensor. These calculations were performed using the NEWTAN software described by Vogt (1990). The calculated reflectance is a standardized value which allows a comparative analysis of values measured by different radiometers. It assumes a Lambertian ground reflectance and is not corrected for atmospheric influences.

The data included 100 relatively cloud- and smoke-free, near-nadir view images that were selected during the July 1987–June 1989 period. The data were geometrically corrected to a master image using the ground control points and accurately coregistered manually. Accurate registration is a key factor for successful detection of nonspurious changes in land-cover (Townshend et al., 1992). The normalized difference vegetation index was calculated from the AVHRR Channels 1 and 2. The atmospheric contamination and directional reflectance effects were reduced from the annual NDVI data series using the maximum value composite technique (Holben, 1986), with a 1-month compositing period. This technique failed to remove all clouds, especially during the rainy season. The August composites for the two years were still largely contaminated by cloud formations and were removed from most of the subsequent analysis. The October composite for the first year had a few remaining clouds in the southwest portion of the scene. It was retained as a way to test the ability of the change vector method to detect cloud contamination in image data and to isolate this purely atmospheric change process from changes in land cover.

Figure 4. Monthly rainfall data at three stations in the Faleme watershed for two hydrological years.

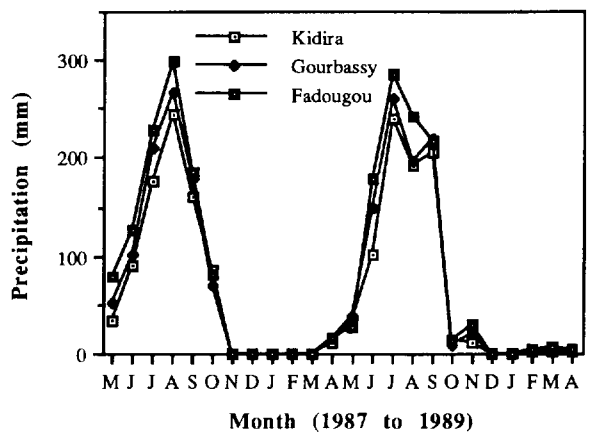

Analytical Procedures

The analysis of the data was performed in three steps. First, the magnitude of the change vector was calculated for a few pixels of known identity. The objective of this preliminary analysis was to compare the quantitative results of the vector analysis with the visual assessment of the interannual changes in temporal development curves. Second, the analysis was extended to the whole image. The magnitude of the interannual change vector was calculated for all pixels. An image of the $|\mathbf{c}(i)|$ values was created and interpreted.

Third, the intrinsic dimensionality of the change vector data was assessed using principal components analysis (PCA) on the set of monthly difference images, which are the components of the change vector image. Given the n-dimensional change vector $\mathbf{c}$,

$$\mathbf{c}(i) = \begin{bmatrix} \mathbf{I}(t_1,y) - \mathbf{I}(t_1,z) \\ \mathbf{I}(t_2,y) - \mathbf{I}(t_2,z) \\ \cdots \\ \cdots \\ \mathbf{I}(t_n,y) - \mathbf{I}(t_n,z) \end{bmatrix}.$$

A linear transformation **A** of the original coordinates is defined to represent the change data with a vector **d** in a new coordinate system,

$$\mathbf{d} = \mathbf{Ac},$$

such that the change data can be represented without correlation in the **d** space or, in other words, such that the covariance matrix of the data in the **d** space (Σ_d) is diagonal. **A** is the transposed matrix of eigenvectors of the covariance matrix of the data in the **c** space (Σ_c). Σ_d is the diagonal matrix of eigenvalues of Σ_c, arranged in order of descending statistical variance accounted for by the principal components (Richards, 1986). In this application of PCA, the original variables are images of the differences between the monthly composited NDVI images from two different years. In a different, but related, application, Townshend et al. (1985) used PCA to explore the underlying dimensionality of multitemporal sets of vegetation index data over a time period shorter than a year. They demonstrated that two dominant directions can be recognized in continental NDVI series: the annualized integrated NDVI and the seasonality of the NDVI. Our analysis is different, in that its goal is to identify the set of main directions of the change vectors in the multidimensional temporal space. These directions correspond to the land-cover change processes affecting the area between the two years.

RESULTS

Preliminary Analysis of Representative Pixels

The NDVI temporal profiles of three pixels, for the two successive hydrological years, is shown in Figure 5. These examples represent different patterns of interannual change. The multitemporal data were composited using a 3-week period. In Figure 5, the NDVI observations are plotted, for each compositing period, at the date of the image for which the maximum NDVI is observed for that pixel. The time-trajectories were produced by linear interpolation of NDVI values between nearest dates. The resulting curves were sampled with a time frequency of 2 weeks to produce 24-dimensional temporal vectors. Table 2 gives, for these three pixels, the magnitude of each change vector and the standard deviation of the components of the change vector, calculated from the digital numbers (0–255). The standard deviation provides a first, rough indication of the direction of the change vector: A large dispersion between the vector components indicates an off-diagonal direction while a low standard deviation indicates a direction near the diagonal.

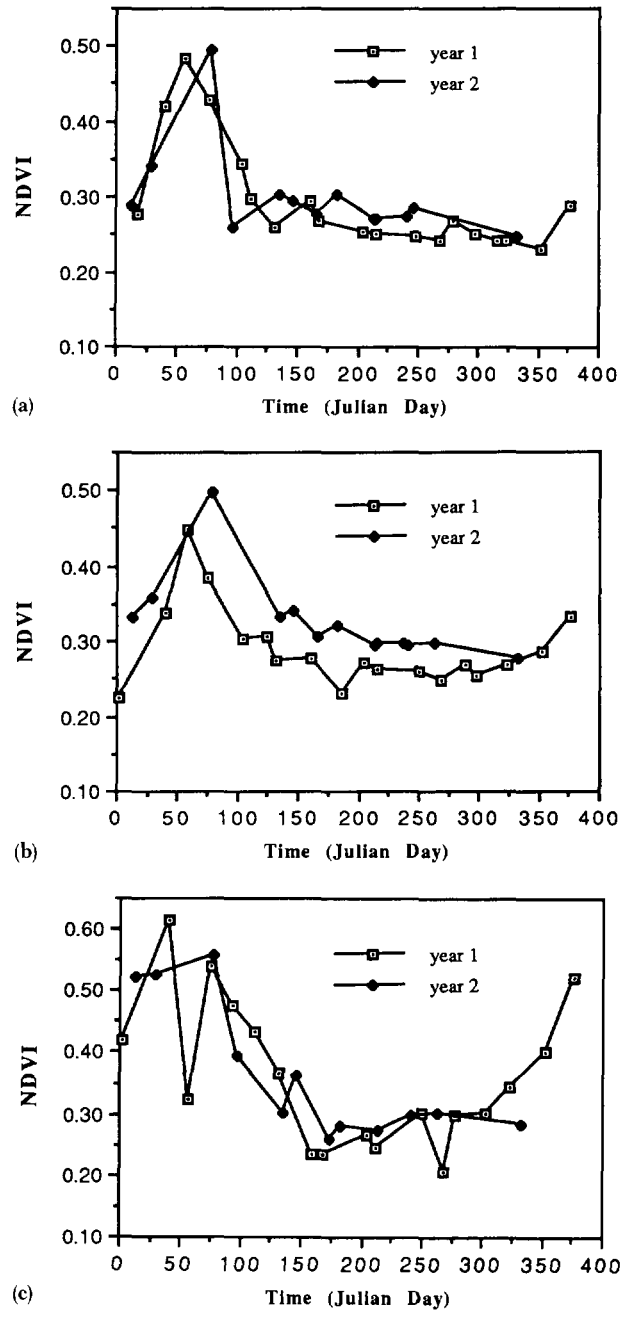

Figure 5. NDVI temporal profiles of three pixels for the two hydrological years: a) savanna (south); b) savanna (southwest); c) herbaceous cover (north).

1. In the first case, a savanna in the south of the scene (Fig. 5a), few changes between the two years can be observed. The only noticeable interannual variations are a later maximum NDVI for the second year and an abrupt decrease of the NDVI at the end of the second rainy season as a result of a fire. The burned surface resulting from this fire could be seen unambiguously on the image from that date. For that pixel, the magnitude of the change vector is low (Table 2). Note that the timing of the early-season shift in the peak val-

Table 2. Magnitude and Direction of the NDVI Change Vector for Three Pixels

Cover Class	*Change in ∫ NDVI*	*Magnitude of Change Vector*[a]	*Change in Temporal Profile*	*Standard Deviation of Change Vector Components*[a,b]
Savanna (south)	Small	39.01	Fire at the end of the rainy season	7.78
Savanna (center)	Lower NDVI curve the first year	84.08	No	12.62
Savanna (north)	Variations in NDVI profile	76.08	Short drought (rainy season) and fire (dry season)	15.71

[a] Calculated from the digital numbers.
[b] Indicates the direction of change vector.

ues may not be accurate since an observation is missing at the begin of the second hydrological year. However, the abrupt decrease in NDVI after the peak of the second year is real.

2. In the second case, a savanna in the southwest of the scene (Fig. 5b), the whole NDVI curve for the first year is lower compared to the second year, suggesting either a lower annual rainfall or the degradation of the vegetation cover at that location. The shapes of the two curves, and therefore the seasonal pattern of vegetation growth, are very similar, with the exception of a small time lag. For this example, the magnitude of the change vector is large compared to the two others.
3. In the third example, an herbaceous cover in the north of the scene (Fig. 5c), the NDVI profile for the first year is characterized by two sharp but short-term declines in NDVI. The first one is probably related to a rainfall shortage during the rainy season, a frequent event in that Sahelian location. The second one occurs as a result of a late fire (mid-March), which can be seen on the image. These variations not only lead to a change in the cumulative value of the NDVI as indicated by the high value of the magnitude of the change vector, but also result in a change in the phenology of the cover, as measured by a higher standard deviation of the vector components.

These empirical observations illustrate the approach and the nature of the multitemporal change vector measurement.

Processing of the Whole Image

For every pixel, the temporal vectors for the two hydrological years, calculated from the monthly composites but excluding the August period, were subtracted from each other, yielding a change vector. The magnitude of this vector was calculated and displayed on an image (Fig. 6). This image provides a cartographic representation of the intensity of land-cover changes between the two years being analyzed. Different threshold values can be defined to separate the areas of significant change from the areas with little or no change, as well as to identify different categories of change based on the magnitude of the interannual variations in NDVI values. In Figure 6, four classes of change intensities can be identified.

Class 1: very bright pixels corresponding to interannual variations in the water level of the Manantali lake, associated with a dam, in the center of the scene, and to some clouds that remained after compositing in the south-west corner of the scene.
Class 2: bright patches at the southern edge of the image which roughly correspond to the ecoclimatic zone characterized by a high annual rainfall.
Class 3: grey tones which occupy a large portion of the image; their interpretation is more difficult since they cover a large portion of the image.
Class 4: darker tones, which correspond to the no-change class.

Note that these four categories of change are distributed in a spatially structured and nonrandom fashion, displaying a high degree of spatial autocorrelation. This suggests that they correspond to real change processes

Figure 6. Image of the magnitude of the change vector.

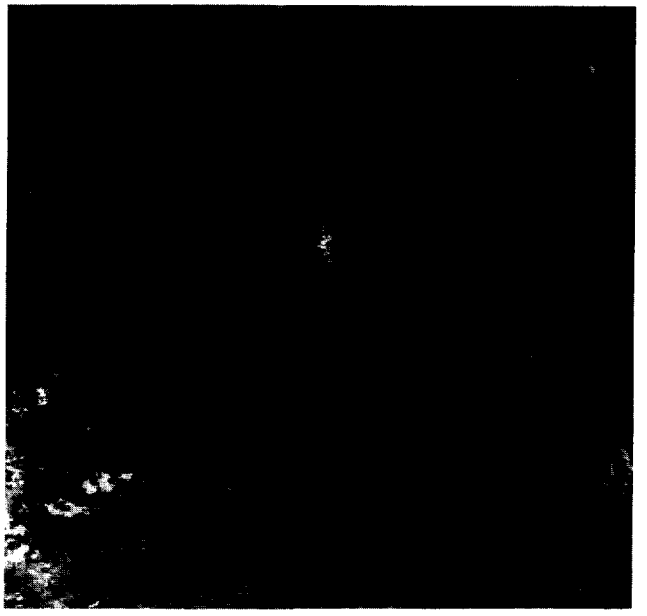

Table 3. Eigenvalues and Percentage of Total Variance Explained by Principal Component Images

Component	*Eigenvalue*	*% Variance*	*Cumulative % Variance*
1	1385.16	30.99	30.99
2	650.98	14.57	45.56
3	479.65	10.73	56.29
4	447.48	10.01	66.30
5	336.92	7.54	73.84
6	303.33	6.79	80.63
7	253.10	5.66	86.29
8	224.65	5.03	91.32
9	166.64	3.73	95.05
10	134.08	3.00	98.05
11	87.36	1.95	100.00

rather than to noise or computation artifacts, which would be spatially unstructured. In order to interpret the meaning of these categories of change intensities, we turn now our attention to the directions of the change vectors in the multitemporal space.

Intrinsic Dimensionality of the Change Vector Image

The PCA calculated on the monthly difference images (excluding the August period) produced unusual results in the sense that 8 out of the 11 principal component images are required to account for more than 90% of the total variance (Table 3). In the work of Townshend et al. (1985) on single-year NDVI time series, only the first two principal component images (out of 8 for Africa and 10 for North America) were required to account for more than 90% of the total variance. Our result underscores the difference in information content between change vectors and time-trajectories. Clearly, interannual change processes are more diverse in their nature, intensity, timing, and duration than seasonal changes.

The principal component images were compared to the monthly difference images with the aid of the factor loadings matrix (Table 4). The analysis of these images and their correlation reveal that each principal component image represents one specific type of change process. Four of these processes, represented by specific components, can be clearly interpreted:

Differences in vegetation growth at the start of the growing season: The first principal component (PC1) is correlated to the May and June compositing periods (Table 4) and represents changes in vegetation growth at the start of the growing season. As the AVHRR data set starts in July, it actually corresponds to the beginning of the next rainy season, at the end of the hydrological year.

Differences in vegetation senescence of tree and shrub savannas: PC2 is correlated to the dry season months: December, January, and, to a lesser extent, February and March compositing periods. It represents differences in the rate of vegetation senescence for the savannas in the south and center of the scene.

Differences in vegetation senescence of grasslands: PC3 is correlated to the November compositing period and represents differences in the rate of senescence of the herbaceous cover that dominates the northern part of the scene.

Differences in haze and cloud contamination: PC4 is correlated to the July compositing period and PC8 to the October composite, both periods contaminated by haze and clouds respectively.

Also, PC7 displays clearly the Selingue lake behind a dam at the southeast corner of the scene, for which year long variations in water level lead to a strong change signal. The meaning of the other components is more difficult to interpret without detailed biophysical data on the area, but they possibly represent change processes of minor spatial extent.

Examples of Interpretation

Even though our goal is essentially methodological, we provide in this section an interpretation of the change patterns revealed by two of the principal component images (PC1 and PC8) in order to evaluate the validity and accuracy of the change vector analysis. This interpretation assumes the existence of strong relationships

Table 4. Factor Loadings Matrix of the PCA

	Jul	*Sep*	*Oct*	*Nov*	*Dec*	*Jan*	*Feb*	*Mar*	*Apr*	*May*	*Jun*
1	−0.398	−0.225	0.063	0.306	0.135	0.601	0.336	0.178	0.135	0.837	0.889
2	−0.202	0.079	−0.085	0.309	0.644	0.540	0.520	0.494	0.244	−0.306	−0.302
3	−0.365	−0.406	−0.279	−0.773	−0.068	0.232	0.178	−0.094	−0.035	0.093	−0.171
4	0.763	−0.037	−0.076	−0.314	0.317	0.065	0.171	0.226	0.309	0.232	0.002
5	0.033	−0.166	−0.526	0.156	0.447	−0.032	−0.219	−0.573	−0.562	0.122	−0.058
6	−0.288	0.390	−0.018	−0.142	0.393	−0.438	0.017	0.177	0.318	0.176	−0.003
7	−0.014	−0.594	−0.329	0.234	−0.132	−0.262	0.221	0.277	0.275	0.078	−0.089
8	−0.023	−0.460	0.691	−0.029	0.266	−0.097	−0.011	−0.110	−0.111	−0.029	−0.002
9	−0.025	−0.172	−0.145	−0.056	0.118	0.059	−0.587	0.181	0.302	−0.162	0.137
10	0.025	−0.033	−0.141	−0.099	0.070	−0.115	0.319	0.021	−0.189	−0.248	0.244
11	0.000	−0.003	−0.007	0.023	0.003	0.016	0.109	−0.428	0.441	−0.050	0.022

between the NDVI, vegetation phenology, and rainfall distribution, which have been very well demonstrated for the Sahel by several studies (Justice et al., 1986; Hielkema et al., 1986; Malo and Nicholson, 1990; Nicholson et al., 1990; Justice et al., 1991).

1. The first principal component represents the change processes taking place during the onset of the rainy season. During that period, variations in timings and rates of vegetation growth can be observed. At the end of the first hydrological year (May and June 1988/89), the rains were abundant early in the season, leading to an early start of the growing season. On the PC1 image (Fig. 7c), a large east–west strip of high PC scores dominates the middle of the image. Since PC1 is positively correlated with the difference images for the months of May and June (0.84 and 0.89, respectively), and since the differences have been calculated by subtracting the second year NDVI images from the first year images, this indicates higher NDVI values for the first year compared to the second year in that part of the image. This interpretation is supported by the visual analysis of the June composite for the two years (Fig. 7a and 7b). Much lower PC1 scores can be observed in the southern part of the PC1 image. This indicates higher NDVI values for the second year, as can be verified in Figures 7a and 7b. For the second year, the wave of vegetation greening, moving northward, reached the southern edge of the scene 1 month later than for the first year. As a result, in that portion of the image, the NDVI reached its peak in June of the second year. In the first year, the NDVI was already declining in June, with the peak in vegetation activity occurring in May. The difference image is therefore negative and appears dark on that portion of the PC1 image, which is positively correlated with the July difference image.
2. The eighth principal component identifies cloud contamination of composited data. It is positively correlated with the October difference image (0.69). In the first year, the October composite

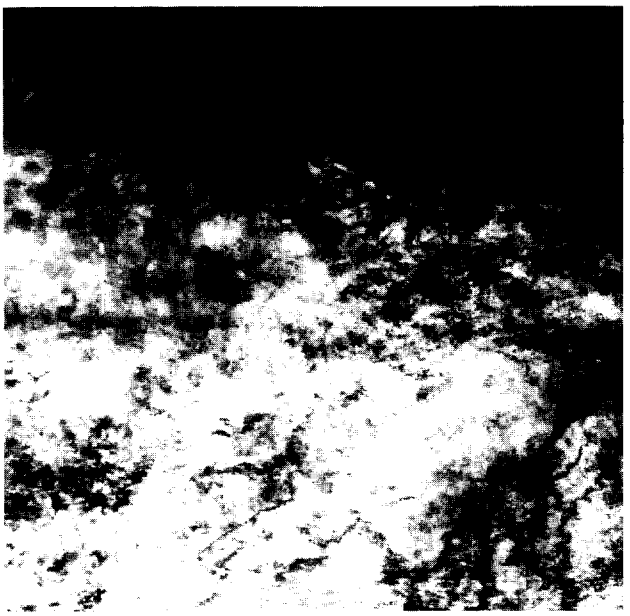

(a)

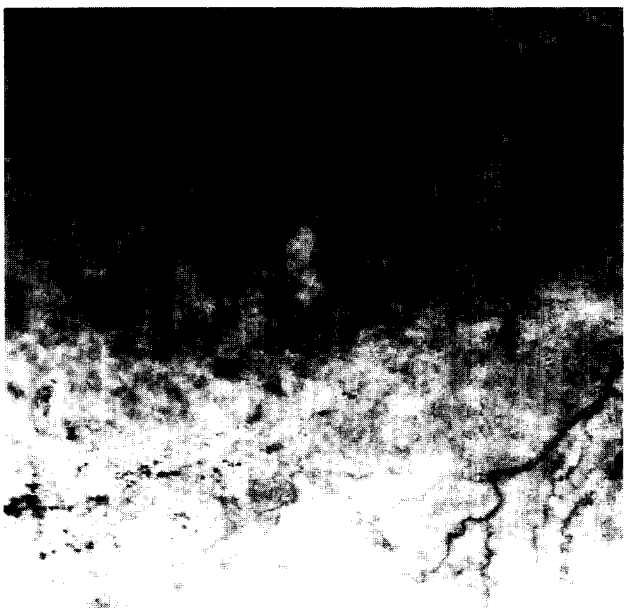

(b)

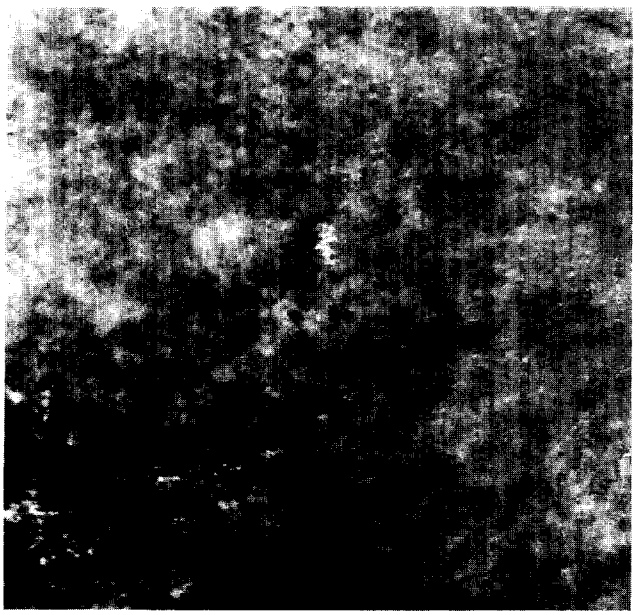

(c)

Figure 7. Interpretation of the first principal component: a) NDVI composited image for June, first hydrological year; b) NDVI composited image for June, second hydrological year; c) image of the first principal component.

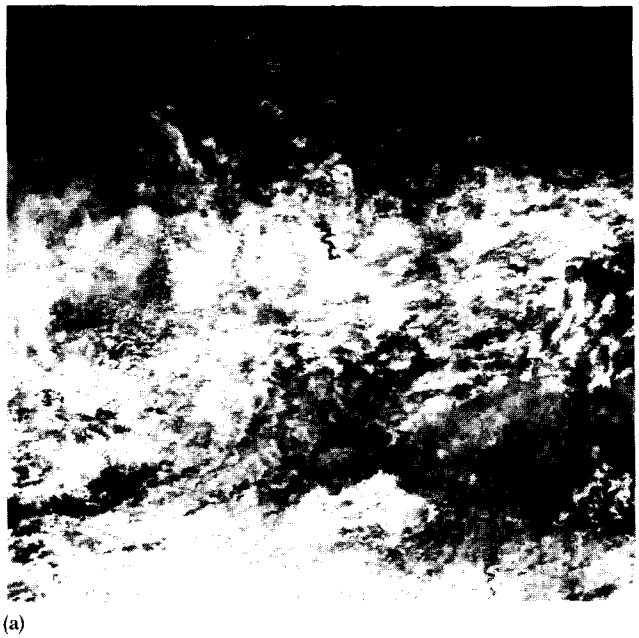

(a)

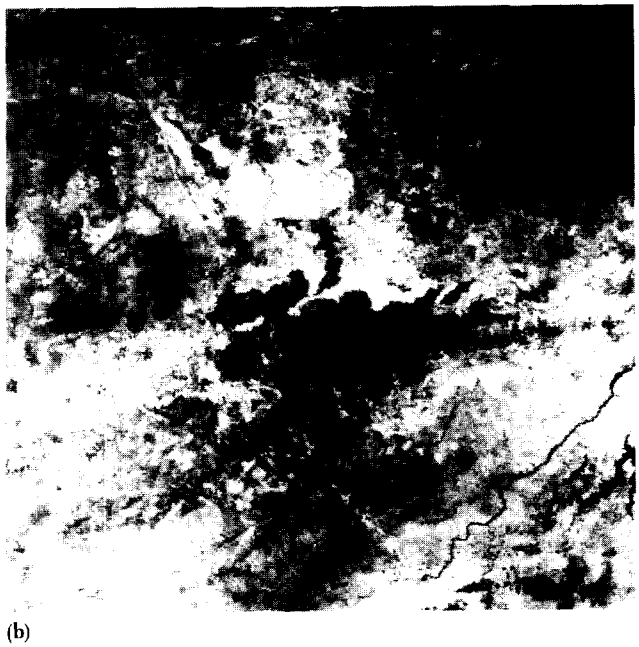

(b)

(c)

Figure 8. Interpretation of the eighth principal component: a) NDVI composited image for October, first hydrological year; b) NDVI composited image for October, second hydrological year; c) image of the eighth principal component.

was contaminated by a string of residual clouds in the southwest part of the scene, while for the second year it was cloud-free (Fig. 8a and 8b). The difference image for October clearly identified this interannual change, which also appears with very high values in the change intensity map (Fig. 6). PC8 isolates the atmospheric contamination of the first year as a separate type of change (Fig. 8c). The clouds appear in black on the composite image since they have a lower NDVI value than the cover type seen in the second year on the same location, which leads to a negative interannual difference.

DISCUSSION

Specific Findings

1. The implicit criteria of categorization of change processes using the multitemporal change vector technique are the timing and duration of the changes. Each principal component accounts for the variance along one specific direction in multidimensional temporal space, defined by a single original axis for short-term changes or by several axis for changes having effects spread over several months.
2. The percentage of the total variance of the change intensity image which is explained by each change process—the rank of each principal component image—depends more on the spatial extent of the change than on the intensity of its effect on the vegetation index. Therefore, the ranking of the principal components is irrelevant to interpret the importance and biophysical meaning of change processes, but is useful to assess the spatial pattern of the change.
3. A primary achievement of change vector analysis is that it is able to isolate the spurious changes caused by residual atmospheric contamination, such as clouds (PCs 4 and 8), from the actual changes in land cover. This decreases reliance on the efficiency of cloud-screening and compositing techniques.
4. Land-cover change caused by biomass burning is

not detected in the analysis of the whole image since the 1-month compositing period masks most of the effects of fires on vegetation. Burned areas have a low NDVI and, therefore, are not selected by the compositing criteria. However, the impact of fires was detected in the analysis of isolated pixels since the compositing period for these profiles was 3 weeks, and the temporal development curves have been sampled with a 2-week frequency. This shows that the change vector analysis is sensitive to the length of the compositing period. Shorter compositing periods will detect shorter-term land-cover changes, such as those related to biomass burning, but will also increase the residual cloud contamination of the data. However, since change vector analysis is able to isolate atmospheric changes, this latter effect might not be a major problem.

Future Work

1. There is some analogy between our research and the well-known Tasseled Cap transformation (Kauth and Thomas, 1976; Crist and Cicone, 1984). This transformation identifies inherent structures present in data from Landsat sensors, which are the expression of physical characteristics of scene classes. Once established, the same transformation coefficients are used for all environments. It would also be desirable to find inherent and stable directions of basic change vectors. With further study across a wider range of ecosystems, it may be possible to define transformations, similar to those of the Tasseled Cap, that quantify specific change processes as they are manifest within the particular rhythm of a particular region. For instance, basic change vectors can be defined: (i) for the dry season, to categorize the transformation of perennial or evergreen vegetation into annual or seasonal vegetation, (ii) for the period of vegetation growth, to identify interannual variations in the date of onset of the rainy season, (iii) for the period of crop harvest, to identify areas of agricultural expansion, (iv) for the burning season, the flooding season, etc. Since the change categorization is largely based on the timing of the change processes within the natural seasonal cycle of the ecosystem, the labeling of specific directions in multitemporal space in terms of change processes will depend on the natural calendar of the ecosystem. For instance, the southern and northern hemisphere will yield opposite interpretations of the directions in the multitemporal space. This factor can, however, be easily controlled by measuring changes on the basis of common seasonal or hydrological cycles rather than on the basis of an absolute calendar. Such an approach should permit replacement of the empirical and scene-dependent nature of PCA by a more universal and ecologically based transformation of multiyear, multitemporal datasets. The definition of fixed transformation coefficients will require the analysis of data sets over a variety of ecosystems.
2. In this article, we have only processed vegetation index data. However, in order to increase the accuracy of the change detection technique, several independent indicators of land cover should be combined in this analysis. In addition to the vegetation index, or any other linear or nonlinear combination of spectral bands in the reflective domain, data in the emissive domain, such as surface temperature, could be integrated. Spatial and angular information can also be considered. For example, patterns of surface spatial structure within various land covers have a rich information content drawn from the natural processes and human activities acting on the land surface. Interannual changes in the seasonal dynamic of the spatial structure of images could therefore be interpreted in terms of land-cover change processes (Lambin and Strahler, 1994).
3. The methodology we present here is being developed as a candidate for the land-cover change product to be provided by NASA's Earth Observing System using the Moderate Resolution Imaging Spectroradiometer (MODIS) (Salomonson et al., 1989). This instrument is similar to the AVHRR sensor in that it provides frequent temporal coverage of the earth, acquiring images on a 2-day repeat. Unlike AVHRR, the instrument images in 36 spectral bands from 0.4 μm to 14 μm selected for studies of atmosphere, ocean, and land. The land bands sample regions of the spectrum that are largely similar to those sampled by the Landsat Thematic Mapper, except that bandwidths are much narrower. Spatial resolution of these bands is 500 m, while resolution of two bands in the red and near-infrared is 250 m. The MODIS instrument will be much better calibrated than AVHRR, and because atmospheric data are acquired simultaneously with land data, it should be possible to routinely correct MODIS land observations for atmospheric effects. MODIS is now scheduled for flight on both EOS-AM and -PM platforms, due for launch in 1998 and 2000, respectively. The land-cover change product is a companion to the land cover product. Both are presently planned to be issued at 3-month intervals and at 1-km spatial resolution. The two products are being developed by the MODIS Land Team. Running et al. (1993) provide a further de-

scription of these and other products planned by the Land Team for MODIS.

CONCLUSION

The change vector analysis, combined with a principal components analysis on the change vectors, has proven to be effective in detecting and categorizing interannual changes between time-trajectories of NDVI data over an area in West Africa. The interpretation of the results of the PCA is scene-dependent and cannot be easily generalized. However, change vector analysis per se allows a more universal interpretation of change processes and can lead to the definition of inherent and stable directions of change. This would require the testing of this technique over a wider variety of ecosystems. The major bottleneck for such a test is the availability of AVHRR LAC / HRPT interannual data series.

Jean-Paul Malingreau and Jean-Marie Grégoire (Joint Research Center, Ispra, Italy) are warmly thanked for providing us with the AVHRR data set they assembled in the framework of the activities of the Monitoring Tropical Vegetation Group. We also thank Joe Lenart, Scott Macomber, and Aaron Moody for their help in processing the data. This work was partially supported by NASA under Contract NAS5-31369 (Earth Observing System).

REFERENCES

Anonymous (1992), Land use and land cover change, *AMBIO* 21:122.

Antonovski, M. Ya., Buchstaber, V. M., and Veksler, L. S. (1991), Application of multivariate statistical analysis for the detection of structural changes in the series of monitoring data, Working Paper WP-91-37, International Institute for Applied Systems Analysis, Laxenburg, Austria, 86 pp.

Badhwar, G. D., and Henderson, H. K. (1985), Application of thematic mapper data to corn and soy-bean development stage estimation, *Remote Sens. Environ.* 17:197–201.

Baret, F., and Guyot, G. (1986), Suivi de la maturation de couverts de blé par radiométrie dans les domaines visible et proche-infrarouge, *Agronomie* 6:27–36.

Belward, A. S., and Lambin, E. F. (1990), Limitations to the identification of spatial structures from AVHRR data, *Int. J. Remote Sens.* 11:921–927.

Box, E. O., Holben, B. N., and Kalb, V. (1989), Accuracy of the AVHRR vegetation index as a predictor of biomass, primary productivity and net CO2 flux, *Vegetatio* 80:71–89.

Cihlar, J., St-Laurent, L., and Dyer, J. A. (1991), Relation between the normalized difference vegetation index and ecological variables, *Remote Sens. Environ.* 35:279–298.

Colwell, J. E., and Weber, F. P. (1981), Forest change detection, in *Proceedings of the 15th International Symposium on Remote Sensing of Environment*, Ann Arbor, MI, Environmental Research Institute of Michigan, Ann Arbor, MI, pp. 839–852.

Crist, E. P., and Cicone, R. C. (1984), A physically-based transformation of Thematic-Mapper data—the TM Tasselled Cap, *IEEE Trans. Géosci. Remote Sens.* GE-22:256–263.

Flitcroft, I. D., Milford, J. R., and Dugdale, G. (1989), Relating point to area average rainfall in semiarid West Africa and the implications for rainfall estimates derived from satellite data, *J. Appl. Meteorol.* 28:252–266.

Goward, S. N., Tucker, C. J., and Dye, D. G. (1985), North American vegetation patterns observed with the NOAA-7 Advanced Very High Resolution Radiometer, *Vegetatio* 64: 3–14.

Goward, S. N., Markham, B., Dye, D. G., Dulaney, W., and Yang, J. (1991), Normalized difference vegetation index measurements from Advanced Very High Resolution Radiometer, *Remote Sens. Environ.* 35:257–277.

Grégoire, J. M. (1990), Effects of the dry season on the vegetation canopy of some river basins of West Africa as deduced from NOAA-AVHRR data, *Hydrol. Sci. J.* 35:323–337.

Hellden, U. (1991), Desertification—time for an assessment? *AMBIO* 20:372–383.

Hellden, U., and Eklundh, L. (1988), National drought impact monitoring. A NOAA NDVI and precipitation data study of Ethiopia, Lund Studies in Geography, Ser. C, No. 15, Lund University Press, Sweden, 55 pp.

Henderson-Sellers, A., and Pitman, A. J. (1992), Land-surface schemes for future climate models: specification, aggregation, and heterogeneity, *J. Geophys. Res.* 97 D3:2687–2696.

Hielkema, J. U., Prince, S. D., and Astle, W. L. (1986), Rainfall and vegetation monitoring in the Savana Zone of the Democratic Republic of Sudan using the NOAA Advanced Very High Radiometer, *Int. J. Remote Sens.* 7:1499–1513.

Holben, B. N. (1986), Characteristics of maximum-value composite images from temporal AVHRR data, *Int. J. Remote Sens.* 7:1417–1434.

IGBP (International Geosphere Biosphere Programme) (1990), *The International Geosphere Biosphere Programme: A Study of Global Change*, The Initial Core Projects Report No. 12, International Council of Scientific Unions, Stockholm, Sweden.

Justice, C. O., Townshend, J. R., Holben, B. N., and Tucker, C. J. (1985), Analysis of the phenology of global vegetation using meteorological satellite data, *Int. J. Remote Sens.* 6: 1271–1318.

Justice, C. O., Holben, B. N., and Gwynne, M. D. (1986), Monitoring East African vegetation using AVHRR data, *Int. J. Remote Sens.* 7:1453–1475.

Justice, C. O., Markham, B. L., Townshend, J. R., and Kennard, R. L. (1989), Spatial degradation of satellite data, *Int. J. Remote Sens.* 10:1539–1561.

Justice, C. O., Dugdale, G., Townshend, J. R., Narracott, A. S., and Jumar, M. (1991), Synergism between NOAA-AVHRR and Meteosat data for studying vegetation development in semi-arid West Africa, *Int. J. Remote Sens.* 12:1349–1368.

Kauth, R. J., and Thomas, G. S. (1976), The Tasselled Cap—a graphic description of the spectral-temporal development of agricultural crops as seen by Landsat, in *Proceedings of the Symposium on Machine Processing of Remotely Sensed Data*, Purdue University, West Lafayette, IN, Purdue University Press, pp. 4B41–4B51.

Lambin, E. F., and Strahler, A. H. (1994), Indicators of land cover change for change-vector analysis in multitemporal space at coarse spatial scales, *Int. J. Remote Sens.*, forthcoming.

Lloyd, D. (1990), A phenological classification of terrestrial

vegetation cover using shortwave vegetation index imagery, *Int. J. Remote Sens.* 11:2269–2279.

Loveland, T. R., Merchant, J. W., Ohlen, D. O., and Brown, J. (1991), Development of a land-cover database for the conterminous U.S., *Photogramm. Eng. Remote Sens.* 57: 1453–1463.

Malila, W. A. (1980), Change vector analysis: an approach for detecting forest changes with Landsat, in *Proceedings of the 6th Annual Symposium on Machine Processing of Remotely Sensed Data*, Purdue University, West Lafeyette, IN, Purdue University Press, pp. 326–335.

Malingreau, J. P. (1986), Global vegetation dynamics: satellite observations over Asia, *Int. J. Remote Sens.* 7:1121–1146.

Malingreau, J. P. (1989), The vegetation index and the study of vegetation dynamics, in *Applications of Remote Sensing to Agrometeorology* (F. Toselli, Ed.), Commission of European Community & European Space Agency, Brussels, pp. 285–303.

Malingreau, J. P., Stephens, G., and Fellows, L. (1985). Remote sensing of forest fires: Kalimantan and North Borneo in 1982–83, *AMBIO* 14:314–321.

Malingreau, J. P., Tucker, C. J., and Laporte, N. (1989), AVHRR for monitoring global tropical deforestation, *Int. J. Remote Sens.* 10:855–867.

Malo, A. D., and Nicholson, S. E. (1990), A study of rainfall and vegetation dynamics in the African Sahel using normalized difference vegetation index, *J. Arid Environ.* 19:1–24.

Mather, J. R., and Sdasyuk, G. V., Eds., (1991), *Global Change. Geographical Approaches*, University of Arizona Press, Tucson, AZ, 289 pp.

Nelson, R., and Holben, B. (1986), Identifying deforestation in Brazil using multiresolution satellite data, *Int. J. Remote Sens.* 7:429–448.

Nicholson, S. E., Davenport, M. L., and Malo, A. D. (1990), A comparison of the vegetation response to rainfall in the Sahel and east Africa using NDVI from NOAA AVHRR, *Climate Change* 17:209–214.

Odenweller, J. B., and Johnson, K. I. (1984), Crop identification using Landsat temporal-spectral profiles, *Remote Sens. Environ.* 14:39–54.

ORSTOM (Institut Francais de Recheche Scientifique pour le Développement en Coopération) (1991), Conséquences hydrologiques des changements d'états de surface survenant sur les basins des grands fleuves d'Afrique de l'Ouest, Final Report of Phases I and II, Contract No. 3840-89-11 ED ISP F, Centre Commun. de Recherche d'Ispra, IATD, Montpellier, France.

Richards, J. A. (1986), *Remote Sensing Digital Image Analysis*, Springer-Verlag, Berlin, 281 pp.

Running, S. W., Justice, C. Salomonson, V., et al. (1994), Terrestrial remote sensing science and algorithms planned for EOS / MODIS, *Int. J. Remote Sens.*, forthcoming.

Salmonson, V. V., Barnes, W. L., Maymon, P. W., Montgomery, H. E., and Ostrow, H. (1989), MODIS: advanced facility instrument for studies of the Earth as a system, *IEEE Trans. Geosci. Remote Sens.* 27:145–153.

Samson, S. A. (1993), Two indices to characterize temporal patterns in the spectral response of vegetation, *Photogramm. Eng. Remote Sens.* 59:511–517.

Sellers, P. (1985), Canopy reflectance, photosynthesis and transpiration, *Int. J. Remote Sens.* 6:1335–1372.

Singh, A. (1989), Digital change detection techniques using remotely-sensed data, *Int. J. Remote Sens.* 10:989–1003.

Stow, D. A., Tinney, L. R., and Estes, J. E. (1980), Deriving land use / land cover change statistics from Landsat: a study of prime agricultural land, in *Proceedings of the 14th International Symposium on Remote Sensing of Environment*, Ann Arbor, MI, Environmental Research Institute of Michigan, Ann Arbor, MI, pp. 1227–1237.

Thomas, G., and Henderson-Sellers, A. (1987), Evaluation of satellite derived land-cover characteristics for global climate modelling, *Climate Change* 11:313–348.

Townshend, J. R. G., Goff, T. E., and Tucker, C. J. (1985), Multitemporal dimensionality of images of Normalized Difference Vegetation Index at continental scales, *IEEE Trans. Geosci. Remote Sens.* GE-23:888–895.

Townshend, J. R., Justice, C. O., and Kalb, V. (1987), Characterization and classification of South American land cover types using satellite data, *Int. J. Remote Sens.* 8:1189–1207.

Townshend, J. R. G., Justice, C., Li, W., Gurney, C., McManus, J. (1991), Global land-cover classification by remote sensing: present capabilities and future possibilities, *Remote Sens. Environ.* 35:243–255.

Townshend, J. R. G., Justice, C. O., Gurney, C., and McManus, J. (1992), The impact of misregistration on the detection of changes in land-cover, *IEEE Trans. Geosci. Remote Sens.* 30(5):1054–1060.

Tucker, C. J., and Sellers, P. J. (1986), Satellite remote sensing of primary production, *Int. J. Remote Sens.* 7:1395–1416.

Tucker, C. J., VanPraet, C., Boerwinkle, E., and Gaston, A. (1983). Satellite remote sensing of total dry matter accumulation in the Senegalese Sahel, *Remote Sens. Environ.* 13:461–474.

Tucker, C. J., Holben, B. N., and Goff, T. E. (1984), Intensive forest clearing in Rondonia, Brazil, as detected by satellite remote sensing, *Remote Sens. Environ.* 15:255–261.

Tucker, C. J., Townshend, J. R., and Goff, T. E. (1985), African land-cover classification using satellite data, *Science* 227: 369–375.

Tucker, C. J., Justice, C. O., and Prince, S. D. (1986), Monitoring the grasslands of the Sahel 1984–1985, *Int. J. Remote Sens.* 7:1571–1581.

Tucker, C. J., Dregne, H. E., and Newcomb, W. W. (1991), Expansion and contraction of the Sahara Desert from 1980 to 1990, *Science* 253:299–301.

Virag, L. A., and Colwell, J. E. (1987), An improved procedure for analysis of change in Thematic Mapper image-pairs, in *Proceedings of the 21st International Symposium on Remote Sens. Environ.*, Ann Arbor, MI, Environmental Research Institute of Michigan, Ann Arbor, MI, pp. 1101–1109.

Vogt, J. (1990), Calculation of t-o-a albedo, NDVI, surface temperature, and precipitable water content of the atmosphere from NOAA AVHRR data, Technical Note 1.90.72, Commission of the European Communities, Joint Research Centre, Ispra, Italy, 29 pp.

Woodwell, G. M., Houghton, R. A., Stone, T. A., Nelson, R. F., and Kovalick, W. (1987), Deforestation in the tropics: new measurements in the Amazon Basin using Landsat and NOAA Advanced Very High Resolution Radiometer imagery, *J. Geophys. Res.* 92(D2):2157–2163.